Communications in Physics, Vol. 35, No. 4 (2025), pp. 389-402
DOI: https://doi.org/10.15625/0868-3166/23365

Study on optical properties and energy transfer of Dy^{3+} ions in ZnS semiconductor nanocrystals

Trinh Thi Thu Huong[1,2], **Nguyen Thi Hien**[2] **and Nguyen Xuan Ca**[2,†]

[1]*Department of Science and Technology, Hanoi University of Industry, Hanoi, Vietnam*
[2]*Institute of Science and Technology, TNU- University of Science, Thai Nguyen, Vietnam*

E-mail: †canx@tnus.edu.vn

Received 17 April 2025; *Accepted for publication 2 July 2025*; *Published 9 December 2025*

Abstract. *In this study, Dy^{3+}-doped ZnS nanocrystals (NCs) with concentrations varying from 0.5-3% were successfully synthesized by the wet chemical method in a pure Ar atmosphere. X-ray diffraction (XRD) and Energy Dispersive X-ray (EDX) results indicated that the material crystallized in a stable cubic phase with a nanometer-sized particle, confirming the presence of elements in the sample. Fourier Transform Infrared (FTIR) spectra recorded characteristic vibrational bands of Zn–S bonds and surface organic functional groups, confirming the formation of ZnS host and a stable organic coating surrounding the nanoparticles. Ultraviolet–Visible (UV-Vis) absorption spectra confirm the quantum confinement effect compared to the ZnS bulk semiconductor. The photoluminescence (PL) spectra of the samples exhibited characteristic emission lines of Dy^{3+}, with the yellow peak at ~580 nm being the most dominant. The CIE color coordinate and correlated color temperature (CCT) analysis results showed the ability to tune the color from cool blue light of pure ZnS to warm white light when doped with Dy^{3+}. The fluorescence quenching that occurred at Dy^{3+} concentrations above 2% and the decrease in fluorescence lifetime with increasing Dy^{3+} concentrations were explained through cross-relaxation energy transfer processes in Dy^{3+} ions. These characteristics demonstrate that ZnS: Dy^{3+} NCs are promising luminescent materials for white light LEDs and advanced optoelectronic applications.*

Keywords: Dy^{3+}; ZnS; nanocrystal; energy transfer; optical properties.
Classification numbers: 78.67.Hc; 78.55.-m; 61.05.cp.

1. Introduction

Zinc sulfide (ZnS) is a group II–VI semiconductor with a wide band gap between ~3.68 eV (cubic) and ~3.8 eV (hexagonal) at room temperature. ZnS exists in two main crystal structures: sphalerite (cubic) and wurtzite (hexagonal), with sphalerite being the most common and stable under ambient conditions [1, 2]. With a size below the Bohr exciton radius (~2.5 nm), ZnS nanocrystals exhibit strong quantum confinement effects, leading to optical and electronic properties that differ significantly from those of the bulk material. This allows for the tuning of the

emission energy by controlling the grain size. ZnS NCs emit light strongly from the ultraviolet to visible region. Due to this property, ZnS NCs are widely used in optical applications such as light-emitting diodes (LEDs), displays, and optical sensors [3, 4]. In addition, ZnS NCs also have high chemical and thermal stability and are low in toxicity. Strong luminescence and high stability make ZnS NCs potential materials in optoelectronic devices, optical sensors, and photocatalytic materials [1, 5, 6].

Rare-earth ions doped in semiconductor NCs combine the quantum properties of nanoparticles with the unique optical properties of rare-earth ions. When rare-earth ions such as Eu^{3+}, Tb^{3+}, Dy^{3+}, or Er^{3+} are doped into semiconductor quantum dots such as ZnS, ZnO, ZnSe, CdS, CdSe, or TiO_2, they can create intermediate energy levels in the band gap of the material [7–9]. This results in strong luminescence with characteristic wavelengths, usually in the visible or near-infrared region, depending on the type of rare-earth ions used. Rare-earth ion doping also improves the luminescence performance of NCs, expanding the range of applications from optoelectronic devices such as light-emitting diodes (LEDs), lasers, to sensors and optical systems [8, 9]. Due to the ability to tune optical properties by changing the type of rare earth ions and doping level, rare earth-doped semiconductor NCs become one of the promising materials for high-tech applications [10–12].

The rare earth ions Dy^{3+} (Dysprosium) are ions with unique optical properties, often used in luminescence applications due to their ability to emit strong light when excited [13]. Dy^{3+} ion has an electron configuration [Xe], in which the 4f electrons are well shielded by the 5s and 5p layers, making the 4f energy levels less affected by the crystal lattice environment. Therefore, the Dy^{3+} ion has a narrow and stable emission spectrum when doped into various materials [14, 15]. The characteristic spectral transitions of Dy^{3+} mainly originate from the excited state $^4F_{9/2}$ to the ground levels of ^6H_J, where: $^4F_{9/2} \rightarrow {}^6H_{15/2}$: strong emission in the yellow–green region; $^4F_{9/2} \rightarrow {}^6H_{13/2}$: emission in the orange–red region. The intensity ratio between these two bands is often used to evaluate the correlated color temperature (CCT) and color rendering index (CRI) in white lighting applications [14, 16]. When Dy^{3+} ions are doped into host materials such as ZnS or other hosts, they exhibit sharp and well-defined luminescence bands with high intensity and remarkable stability, showing minimal dependence on environmental conditions [17]. The emission spectrum of the resulting material is multi-band: Combining blue, yellow, and red emissions to produce near-white light. Dy^{3+} doping in ZnS NCs not only introduces 4f levels into the band gap but also couples with surface defect states, thereby broadening emission features and enabling control over quantum efficiency. This makes ZnS:Dy^{3+} a potential material for applications in white light LEDs, optical sensors, and biofluorescent markers [17].

In this paper, we synthesized and studied the optical properties and energy transfer process of Dy^{3+} ions in ZnS host materials. The structural, compositional, lattice vibrational, and optical properties were characterized by XRD, EDX, FTIR, UV-Vis, PL, and fluorescence decay spectra. The effect of Dy^{3+} concentration on the optical properties of the material has been studied in detail.

2. Experiment

2.1. Materials

ZAT (Zinc acetate-$Zn(CH_3COO)_2.2H_2O$, 99.99%), OLA (Oleylamine -$C_{18}H_{37}N$, 97%), ODE (1-Octadecene- $CH_3(CH_2)_{15}CH{=}CH_2$, 95%), TOP (tri-n-octylphosphine - $C_{24}H_{51}OP$ 97%),

DyAT (Dysprosium acetate dihydrate ($Dy(CH_3COO)_2$-$2H_2O$); Isopropanol (70 %), and Toluene (99.8%) were purchased from Sigma–Aldrich. All reactions to prepare NCs were carried out in an ultra-clean Ar atmosphere (99.995%).

2.2. Fabrication of Dy^{3+}-doped ZnS nanocrystals

Dy^{3+}-doped ZnS NCs (ZnS:Dy^{3+}) were synthesized by a wet chemical method in a pure Ar atmosphere. First, zinc precursor (ZAT) and Dy^{3+} salt (DyAT) were accurately weighed according to the desired Dy^{3+}/Zn_2^+ molar ratio and dissolved in a solvent mixture of tri-n-octylphosphine (TOP) and 1-octadecene (ODE) in a three-necked flask. The mixture was vigorously stirred and continuously bubbled with Ar gas to completely remove oxygen and moisture. Then, oleylamine (OLA) was slowly added into the system as a complexing agent and surface stabilizer. The solution was heated to 260˚C and maintained at this temperature for 60 min to form ZnS:Dy^{3+} NCs. After the reaction, the solution was cooled naturally to room temperature. The product was collected by centrifugation, washed several times with isopropanol and toluene to remove organic impurities, and then dried under vacuum. The samples were named according to the Dy^{3+} concentration: ZnS, ZnS: Dy^{3+}0.5%, ZnS: Dy^{3+}1%, ZnS: Dy^{3+}2%, and ZnS: Dy^{3+}3%.

2.3. Characteristic measurements

The structures of the NCs were investigated by XRD. The measurements were performed on a SIMENS D5005 X-ray diffractometer (Bruker) with Cu-Kα radiation (λ = 0.154 nm). The Raman spectra (RS) of the dried samples were measured using a LABRAM-HR800 spectrometer (Jobin Yvon) operating at λ=488 nm (2.54 eV). The elemental composition of the samples was analyzed using energy dispersive X-ray spectroscopy (EDX, Model JOEL JSM-5610). The UV-Vis absorption spectra of the NCs were recorded using a Jasco V-770 spectrophotometer (Varian). The PL spectra and the decay time curves were measured using an FLS1000 system with a 450 W Xe excitation source. All measurements were performed at room temperature.

3. Results and discussion

3.1. Study of structure and composition

The X-ray diffraction (XRD) patterns of ZnS and ZnS: Dy^{3+} NCs are shown in Fig. 1. The observed diffraction peaks correspond to the lattice planes (111), (200), (220), (311), (400), which are consistent with the cubic standard card (JCPDS No. 05-0566). This result demonstrates that the fabricated NCs all have cubic structures belonging to the space group F-43m [18, 19].

Compared with undoped ZnS NCs, the diffraction peaks of Dy^{3+}-doped ZnS NCs shifted slightly toward smaller 2θ angles with increasing Dy^{3+} concentration, indicating an increase in the crystal lattice constant. This slight shift is due to the replacement of small radius Zn ions (0.74 Å) by larger radius Dy^{3+} ions (0.912 Å) [20]. This replacement causes internal stress in the material and shifts the diffraction peaks toward smaller 2θ angles. The shift of the diffraction peaks toward smaller 2θ angles with increasing Dy^{3+} concentration indicates that Dy^{3+} ions have replaced the positions of Zn ions. The incorporation of Eu^{3+} ions into ZnS NCs introduces lattice strain, which was evaluated using the Stokes–Wilson relation ($\varepsilon = \beta.\cos\theta/4$) [21], and the results are summarized in Table 1. The crystallite size (D) of the NCs can be determined using the Debye–Scherrer equation from the X-ray diffraction line broadening [22]

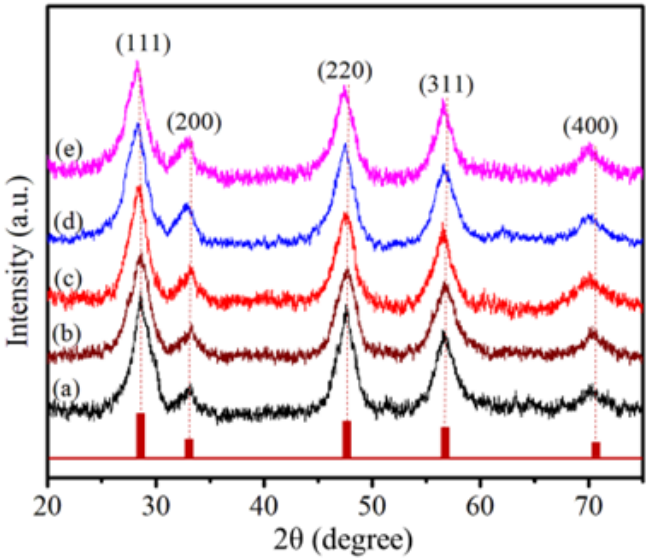

Fig. 1. X-ray diffraction pattern of: ZnS (a), ZnS:Dy^{3+}0.5% (b), ZnS:Dy^{3+}1% (c), ZnS:Dy^{3+}2% (d), and ZnS:Dy^{3+}3% (e).

$$D = \frac{k\lambda}{\beta \cos\theta}, \tag{1}$$

where λ = 1.54 Å is the wavelength of X-ray, k=0.9, θ is the Bragg diffraction angle and β is the width of the diffraction line. The lattice constant (a) of the ZB-structured NCs was determined using the [111] orientation. The relationship between the lattice constant (a) and the distance between planes (d_{hkl}) is given by the following equation [22, 23]:

$$\frac{1}{d_{hkl}^2} = \frac{h^2 + k^2 + l^2}{a^2}, \tag{2}$$

where h, k, and l are Miller indices corresponding to the crystallographic planes. d_{hkl} is the interplanar spacing, was calculated using Bragg's equation [22, 23]:

$$n\lambda = 2d_{hkl} \sin\theta. \tag{3}$$

Here, n is integer, λ is the X-ray wavelength, and θ is the diffraction angle. The parameters, including crystallite size (D), lattice constant (a), and interplanar spacing (d_{hkl}), were calculated and are listed in Table 1.

The chemical compositions of ZnS and ZnS: Dy^{3+}3% NCs were analyzed by energy dispersive X-ray (EDX) spectroscopy, and the results are shown in Fig. 2. The presence of Zn, O, Dy, and C elements in the sample can be seen. The presence of the C element is due to the organic compounds used in the fabrication of the NCs. The EDX spectrum of the ZnS NCs shows characteristic lines S-K_α (~2.31 keV) and Zn-K_α (~8.64 keV) [24]. For the ZnS:Dy^{3+} sample, in addition to the peaks of Zn and S, the appearance of the L_α (~6.49 keV) and L_β (~7.34 keV) lines of Dy^{3+} ions was also observed, confirming the presence of Dy^{3+} ions in the sample.

Table 1. Crystal lattice parameters of the NCs.

Sample	$2\theta_{111}$ **(deg.)**	β **(deg.)**	d_{hkl} **(nm)**	a **(Å)**	D **(nm)**	$\varepsilon \times 10^{-3}$
ZnS	28.547	2.434	3.141	5.441	3.16	10.29
ZnS: Dy^{3+} 0.5%	28.485	2.598	3.146	5.449	2.96	10.98
ZnS: Dy^{3+} 1%	28.393	2.401	3.151	5.457	3.21	10.15
ZnS: Dy^{3+} 2%	28.238	2.501	3.155	5.465	3.08	10.58
ZnS: Dy^{3+} 3%	28.202	2.575	3.166	5.483	2.99	10.89

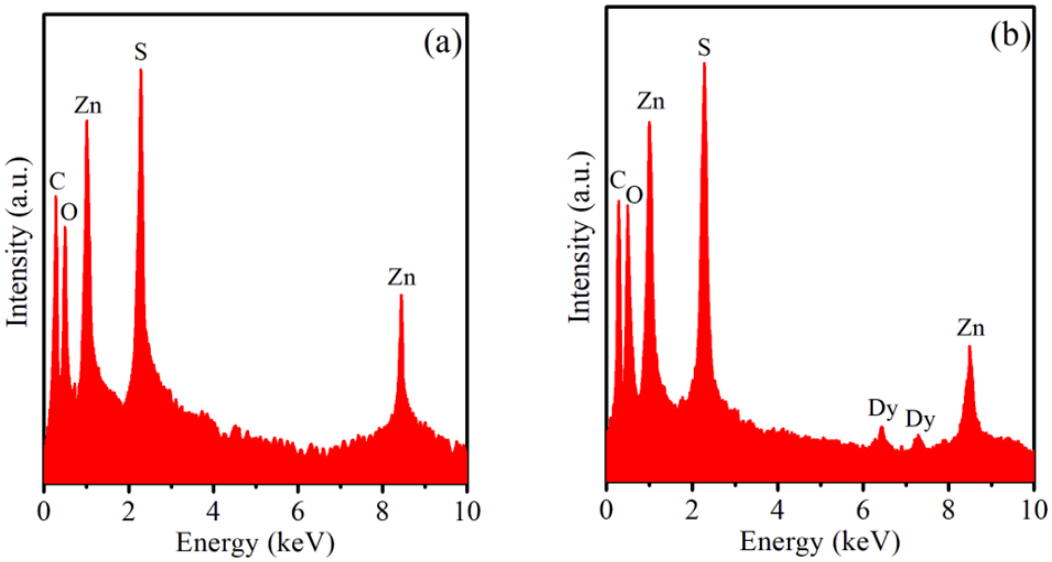

Fig. 2. EDX spectra of ZnS (a) and ZnS: Dy^{3+}3% (b) NCs.

3.2. Vibration properties

The Fourier transform infrared (FT-IR) spectra of ZnS: Dy^{3+} NCs (Fig. 3) show characteristic absorption bands related to the ZnS host and the organic groups covering the particle surface. The band at around 600–700 cm^{-1} is the Zn–S bond valence vibration, confirming the formation of the ZnS phase [25]. The peaks at ~1050 cm^{-1} (C–O–C) and ~1392–1426 cm^{-1} (C–O) correspond to the ether/alkoxy group and carboxylate group valence vibrations of the surfactant, respectively [25, 26]. Notably, the C–O band shifts from 1426 cm^{-1} (undoped sample) to ~1392 cm^{-1} (Dy^{3+} doped sample at 3% concentration), indicating a change in the doping environment due to the stronger interaction of the carboxylate group with the metal centers at the surface in the presence of Dy^{3+}. The band at 1556 cm^{-1} is the C=O valence vibration, while the peaks at 2970 cm^{-1} (C–H) and the broad band 3200–3600 cm^{-1} (O–H) are characteristic of the C–H vibration of the alkyl chain and hydroxyl groups or water adsorbed on the surface, respectively [26]. The distinct presence of C–H, C–O–C, and C=O bands suggests that the organic layer still exists, playing a role in stabilizing the nanoparticles and limiting aggregation. The strong O–H band reflects a hydroxyl-rich surface, which is likely to participate in charge trapping processes, thereby

affecting the optical properties of the material [27]. The organic ligands present on the surface of ZnS:Dy^{3+} NCs can strongly influence their luminescence efficiency. On the one hand, these ligands stabilize the nanocrystals and reduce non-radiative losses caused by aggregation. On the other hand, functional groups such as –OH or –COOH may introduce surface trap states that act as quenching centers or compete with Dy^{3+} ions for excitation energy. Consequently, the balance between surface passivation and trap-assisted quenching plays a decisive role in determining the overall optical performance of the NCs. Comparison of spectra between samples shows that the intensity and width of the Zn–S band change with increasing Dy^{3+} concentration, suggesting local lattice distortion due to Dy^{3+} ions partially replacing Zn_2^+ sites or forming lattice defects. The substitution of Dy^{3+} ions (with a larger ionic radius and higher valence state) for Zn_2^+ in the ZnS lattice inevitably induces local charge imbalance. To maintain charge neutrality, several compensation mechanisms may take place. A common mechanism is the formation of sulfur vacancies (V_S), which readily appear in ZnS and can act as defects to trap charges. The generation of these defects not only restores charge balance but also directly modifies the energy levels, charge transport, and luminescence dynamics, thereby exerting a strong influence on the optical properties of ZnS:Dy^{3+} NCs.

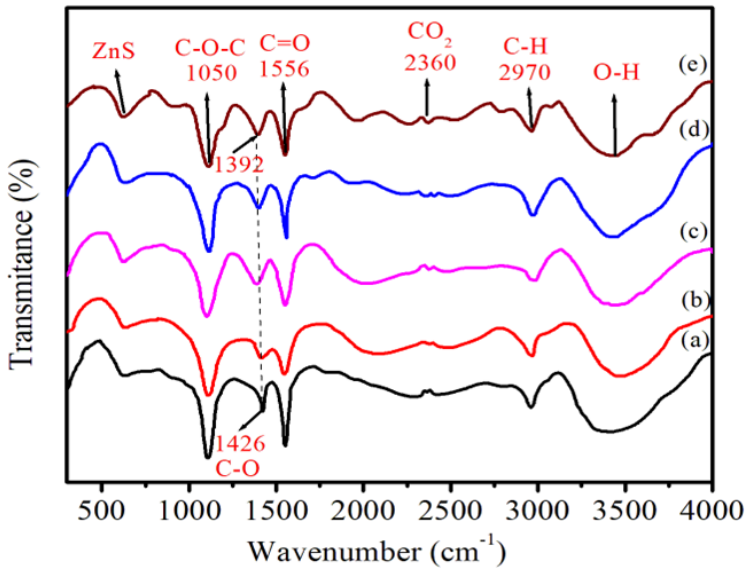

Fig. 3. FT-IR spectra of the NCs: ZnS (a), ZnS:Dy^{3+}0.5% (b), ZnS:Dy^{3+}1% (c), ZnS:Dy^{3+}2% (d), and ZnS:Dy^{3+}3% (e).

The FT-IR spectra confirm the formation of the ZnS phase and the presence of an organic surface layer that stabilizes the nanocrystals and suppresses aggregation. The shift of the C–O band, together with the changes in the intensity and width of the Zn–S band, indicates that Dy^{3+} incorporation modifies the local bonding environment and induces lattice distortions. Moreover, the pronounced O–H vibrations suggest a hydroxyl-rich surface capable of participating in charge-trapping processes, thereby influencing the optical properties of the material.

4. Optical properties

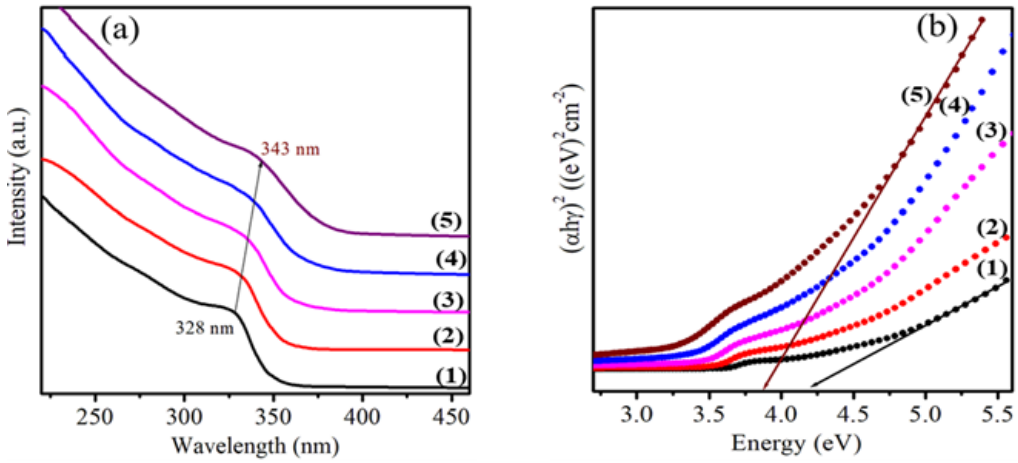

Fig. 4. (a) UV-vis spectra of NCs: ZnS (1), ZnS:Dy^{3+}0.5% (2), ZnS:Dy^{3+}1% (3), ZnS:Dy^{3+}2% (4), and ZnS:Dy^{3+}3% (5); (b) Dependence of $(\alpha hv)^2$ on energy (hv) of Dy^{3+}-doped ZnS NCs.

Fig. 4a shows the UV–Vis absorption spectra of ZnS and ZnS:Dy^{3+} NCs. For undoped ZnS NCs, a distinct absorption peak is observed at 328 nm, which corresponds to the electronic transition from the valence band to the conduction band, commonly referred to as excitonic absorption [1, 8]. When Dy^{3+} is doped, the UV–Vis spectral peak shifts to longer wavelengths as the Dy^{3+} concentration increases, indicating the change in band gap energy and the influence of Dy^{3+} ions on the electronic structure of the host material. The red-shift observed in the UV–Vis absorption spectra of ZnS:Dy^{3+} can be attributed to two main factors. First, since the ionic radius of Dy^{3+} (0.912 Å) is larger than that of Zn^{2+} (0.74 Å) [20], its substitution induces lattice distortion and simultaneously introduces impurity levels within the band gap. These additional states serve as intermediate energy levels, thereby reducing the excitation energy required for electronic transitions and causing a red shift of the absorption edge toward longer wavelengths. Furthermore, the interaction between Dy^{3+} ions and surface defects enhances the density of electronic states, thereby reinforcing the red-shift effect. Second, at higher Dy^{3+} concentrations, the nanocrystal size tends to increase, leading to a weakening of the quantum confinement effect and a consequent narrowing of the band gap. The combined influence of these two mechanisms accounts for the pronounced red-shift behavior observed in ZnS:Dy^{3+} nanocrystals [20].

The optical band-gap energies (E_g) of undoped ZnS and Dy^{3+}-doped ZnS NCs were evaluated by extrapolating the linear portion of the $(\alpha hv)^2$ versus photon energy (hv) plots (Fig. 4b). This analysis is based on the Tauc relation [28]:

$$\alpha hv = A(hv - E_g)^n, \tag{4}$$

where A is a constant, hv is the photon energy, E_g is the optical band gap, h is Planck's constant, α is the absorption coefficient, and n takes different values (2, 3, 1/2, 1/3) corresponding to indirect allowed, indirect forbidden, direct allowed, and direct forbidden transitions, respectively. Since

ZnS is a direct band gap semiconductor ($n = 1/2$), E_g was determined by extrapolating the linear region of the $(\alpha h\nu)^2$ versus $h\nu$ plots to intersect the energy axis.

As shown in Fig. 4b and Table 2, the optical band gap of undoped ZnS NCs is estimated to be ~4.21 eV. Upon incorporation of Dy^{3+} ions, the band-gap energy decreases progressively with increasing Dy^{3+} concentration, from 4.13 eV at Dy^{3+} 0.5% to 3.87 eV at Dy^{3+} 3%. The reduction in band gap of Dy^{3+}-doped ZnS NCs relative to the undoped sample can be attributed to several factors, including lattice strain induced by the larger ionic radius of Dy^{3+} compared to Zn_2^+, the introduction of Dy^{3+}-related impurity states within the band gap, the generation of additional defects, and the weakening of the quantum confinement effect due to the increase in QD size. The size of the NCs can be determined from the energy of the exciton absorption peak according to the equation [29]:

$$E_{NC} = E_{bulk} + \frac{\hbar^2\pi^2}{2R^2}\left(\frac{1}{m_e^*} + \frac{1}{m_h^*}\right) - \frac{1.8e^2}{4\pi\varepsilon_0\varepsilon_r R}. \quad (5)$$

Here, E_{NC} is the band gap energy of a ZnS NC with radius R. E_{bulk} is the band gap energy of bulk ZnS ($\approx$ 3.68 eV for cubic structure). $\hbar$ is the reduced Planck's constant. m^*_e is the effective mass of the electron in ZnS ($m^*_e \approx 0.28\ m_0$, where m_0 is the free electron mass). m^*_h is the effective mass of the hole in ZnS ($m^*_h \approx 0.59\ m_0$). ε_0 is the permittivity of free space, ε_r is the relative permittivity of ZnS ($\varepsilon_r \approx 8.3$), and e is the elementary charge [29]. The average sizes of the ZnS and ZnS:Dy^{3+} NCs estimated from this relation are summarized in Table 2.

Table 2. Absorption peak, band gap and radius of NCs.

Sample	Absorption peak (nm)	Bandgap (eV)	R (nm)
ZnS	328	4.21	1.93
ZnS: Dy^{3+} 0.5%	332	4.13	2.10
ZnS: Dy^{3+} 1%	335	3.98	2.57
ZnS: Dy^{3+} 2%	339	3.92	2.87
ZnS: Dy^{3+} 3%	343	3.87	3.23

The emission spectra of ZnS and ZnS: Dy^{3+} NCs are observed in Fig. 5. The emission spectrum of ZnS NCs (excited at 275 nm) has two narrow and broad emission peaks. The narrow emission peak at 382 nm with high intensity is the emission due to the recombination of electrons in the conduction band with holes in the valence band of ZnS (also known as exciton recombination) [1,6]. The half-width of this peak depends on the size distribution of ZnS NCs; if the particle sizes are more uniform, the half-width of the spectrum will be smaller and vice versa. The broad emission peak at 556 nm with weak intensity is the emission of surface states and defects in ZnS NCs.

The emission spectra of ZnS NCs doped with Dy^{3+} ions with different concentrations all have six emission peaks. These six peaks are characteristic emissions of Dy^{3+} ions. These emissions include: 461 nm ($^4I_{15/2} \rightarrow ^6H_{15}/2$, blue), 484 nm ($^4F_{9/2} \rightarrow {}^6H_{15/2}$, blue), 540 nm ($^4I_{15/2} \rightarrow {}^6H_{13/2}$, green), 580 nm ($^4F_{9/2} \rightarrow {}^6H_{13/2}$, yellow), 665 nm ($^4F_{9/2} \rightarrow {}^6H_{11/2}$, red), and 756 nm ($^4F_{9/2} \rightarrow {}^6H_{9/2}$, infrared). Of these, the emission at 580 nm is the most intense. This emission often greatly affects the emission of Dy^{3+} ions and is called the "hypersensitive transition" [12,13]. Therefore, its intensity is greatly affected by the nature of the environment surrounding the Dy^{3+}

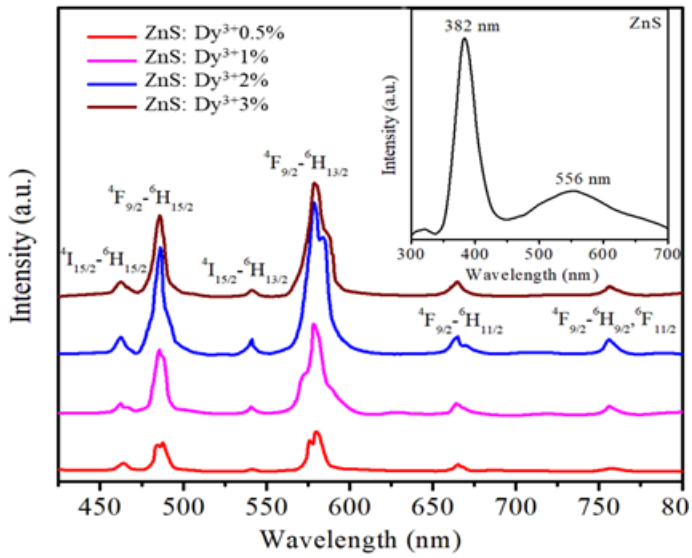

Fig. 5. PL spectra of Dy^{3+}-doped ZnS NCs under 350 nm excitation wavelength.

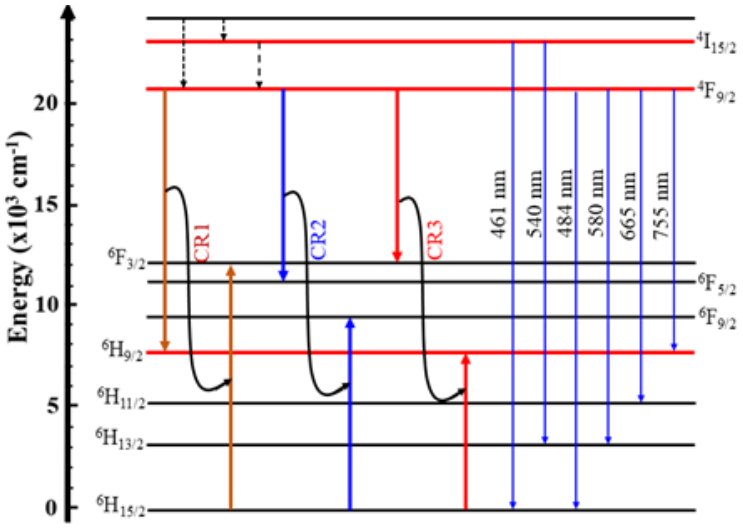

Fig. 6. Energy band structure and energy transfer channels in ZnS: Dy^{3+} NCs.

ions. When the concentration of Dy^{3+} ions increases, the emission intensity increases and reaches a maximum at 2%, and when the concentration of Dy^{3+} continues to increase, the intensity decreases. This is called concentration-induced fluorescence quenching. This phenomenon is often attributed to a reduction in the average distance between Dy^{3+} ions, which enhances the probability of non-radiative interactions such as cross-relaxation (CR) and ion–ion energy transfer, ultimately resulting in a decrease in luminescence intensity.

At high Dy^{3+} concentrations, the reduction in luminescence intensity is attributed to concentration quenching governed by cross-relaxation (CR) mechanisms, as illustrated in Fig. 6. In this process, an excited Dy^{3+} ion at the $^4F_{9/2}$ state can transfer part of its energy to a neighboring Dy^{3+} ion residing in the ground state. The coupled ions subsequently relax through non-radiative channels, predominantly via multi-phonon emission or infrared transitions, thereby reducing the overall radiative efficiency. For ZnS:Dy^{3+} NCs, several possible CR pathways have been identified (Fig. 6), including: CR1: $(^4F_{9/2} \rightarrow {}^6F_{9/2}) \rightarrow (^6H_{15/2} \rightarrow {}^6F_{3/2})$, CR2: $(^4F_{9/2} \rightarrow {}^6F_{5/2}) \rightarrow (^6H_{15/2} \rightarrow {}^6F_{9/2})$, and CR3: $(^4F_{9/2} \rightarrow {}^6F_{3/2}) \rightarrow (^6H_{15/2} \rightarrow {}^6F_{9/2})$. These cross-relaxation channels account for the observed decrease in emission intensity at high Dy^{3+} doping levels [12–14].

4.1. CIE Color Coordinates and Lifetime of the $^4F_{9/2} \rightarrow {}^6H_{13/2}$ (580 nm) transition

The emission properties of the samples were analyzed within the CIE 1931 color space, which describes chromaticity based on the human visual response. The (x, y) chromaticity coordinates of ZnS:Dy^{3+} NCs were calculated from the photoluminescence spectra and plotted on the CIE 1931 diagram, as presented in Fig. 7.

The correlated color temperature (CCT) of the samples was evaluated using McCamy's empirical approximation [22, 23]:

$$CCT = -449n^3 + 3525n^2 - -6823n + 5520.33, \tag{6}$$

where n is defined as $n = (x - x_e)/(y - y_e)$, with $x_e = 0.332$ and $y_e = 0.186$. The calculated CCT values for the ZnS:Dy^{3+} NCs are summarized in Table 3.

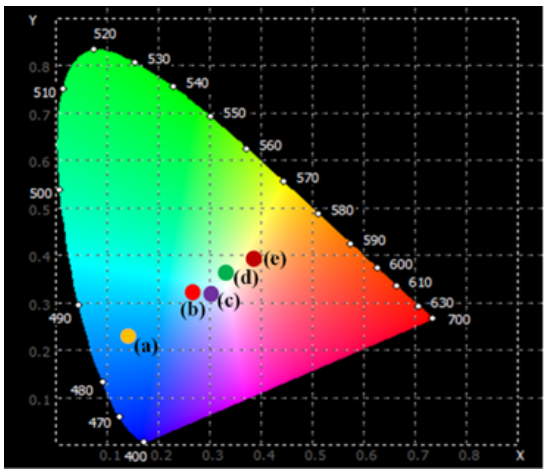

Fig. 7. CIE color coordinates of Dy^{3+}-doped ZnS NCs at λ_{exc} = 350 nm.

The data in Table 3 show a significant change in the chromaticity coordinates (x, y) and correlated color temperature (CCT) with increasing Dy^{3+} concentration in ZnS. The ZnS NCs exhibit chromaticity coordinates of (0.147, 0.239), which are located near the blue emission region on the CIE diagram. It has a very high correlated color temperature (CCT) of 16,731 K, corresponding to

Table 3. Color coordinates and correlated color temperatures of Dy^{3+}-doped ZnS NCs.

Sample	*x*	*y*	**CCT (K)**
ZnS	0.147	0.239	16731
ZnS: Dy^{3+} 0.5%	0.262	0.327	6524
ZnS: Dy^{3+} 1%	0.301	0.313	5815
ZnS: Dy^{3+} 2%	0.341	0.367	5107
ZnS: Dy^{3+} 3%	0.387	0.390	4910

the characteristic cold blue emission of ZnS materials. When Dy^{3+} is doped, the emission spectrum of the sample gradually shifts to the warm yellow–white region due to the strong contribution of the $4F_{9/2} \rightarrow 6H_{13/2}$ transition ($\approx$ 580 nm, yellow).

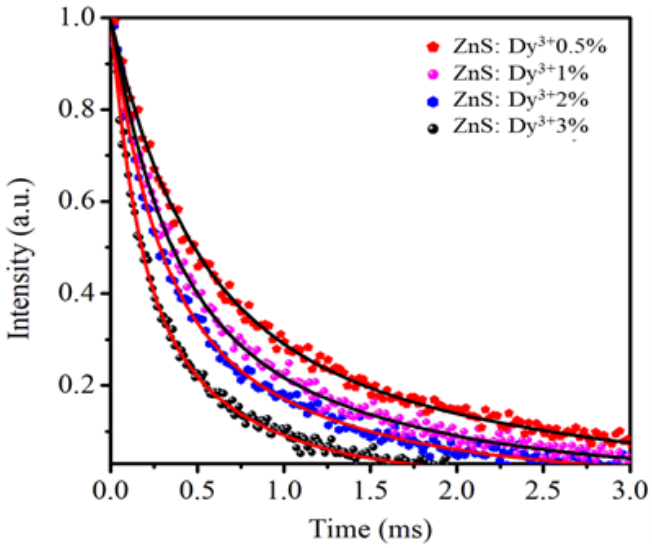

Fig. 8. (Color online) Time-resolved fluorescence curves of Dy^{3+}-doped ZnS NCs measured at 580 nm ($^4F_{9/2} \rightarrow {}^6H_{13/2}$).

At low concentrations (Dy^{3+} 0.5%), the chromaticity coordinates (0.262, 0.327) moved closer to the neutral white region, with the CCT decreasing to 6524 K. At concentrations of 1–2%, the chromaticity coordinates continued to shift towards an increased red–yellow component, with the CCT decreasing to 5815 K and 5107 K, corresponding to warm white light. At Dy^{3+} 3%, the chromaticity coordinates reached (0.387, 0.390) with a CCT of only 4910 K, falling in the warm white region near orange-yellow. This result demonstrates a relative balance between blue (484 nm) and yellow (580 nm) emissions with increasing Dy^{3+} concentration. At low concentrations, both emission bands are present, producing near-white light. As the concentration increases, the cross-relaxation mechanism reduces the blue emission and enhances the yellow/red emission, resulting in a color shift towards the warm white region.

Photoluminescence (PL) decay analysis is a powerful tool in materials science, particularly for investigating rare-earth-doped semiconductors. This technique provides insights into the

excited-state dynamics of luminescent centers and yields valuable information regarding the electronic structure, energy transfer pathways, and defect-related nonradiative processes in the host lattice. Fig. 8 presents the PL decay profiles of the $^4F_{9/2} \rightarrow {}^6H_{13/2}$ transition (~580 nm) of Dy^{3+} ions in all ZnS:Dy^{3+} NCs. The PL decay curves were analyzed using a bi-exponential function, expressed as [1, 22]:

$$I(t) = I_0 + A_1 e^{-\frac{t}{\tau_1}} + A_2 e^{-\frac{t}{\tau_2}}, \tag{7}$$

where *I(t)* is the PL intensity at time *t*, I_0 is the initial intensity at *t*=0, A_1 and A_2 are the pre-exponential factors associated with the two decay channels, and τ_1, τ_2 are their respective lifetimes. The application of a bi-exponential model suggests the coexistence of two major recombination pathways, typically radiative and non-radiative. The average lifetime $\langle\tau\rangle$ was calculated according to the following relation [1, 22]:

$$\langle\tau\rangle = \frac{A_1\tau_1^2 + A_2\tau_2^2}{A_1\tau_1 + A_2\tau_2}. \tag{8}$$

The fitting parameters A_i, τ_i, and the corresponding average lifetimes $\langle\tau\rangle$ for all samples are summarized in Table 4.

Table 4. The constants of time-resolved fluorescence curves of Dy^{3+}-doped ZnS NCs.

Sample	τ_1 **(ms)**	A_1	τ_2 **(ms)**	A_2	$\langle\tau\rangle$ **(ms)**
ZnS: Dy^{3+} 0.5%	0.12	0.34	0.81	0.66	0.76
ZnS: Dy^{3+} 1%	0.10	0.29	0.60	0.71	0.57
ZnS: Dy^{3+} 2%	0.07	0.36	0.48	0.64	0.45
ZnS: Dy^{3+} 3%	0.04	0.32	0.29	0.68	0.27

As seen in Table 4, the average lifetime gradually decreases from 0.76 ms in the ZnS:Dy^{3+}0.5% sample to 0.27 ms in the ZnS:Dy^{3+} 3% NCs. The shorter average lifetime indicates faster non-radiative recombination or more efficient energy transfer processes, meaning that as the Dy^{3+} concentration increases, the ZnS host material transfers energy more efficiently to the Dy^{3+} ions. This accelerates the fluorescent decay, resulting in a shorter lifetime. The decrease in $\langle\tau\rangle$ with increasing Dy^{3+} concentration provides clear evidence of the energy transfer from the ZnS host to the Dy^{3+} ions [16, 23]. As the Dy^{3+} concentration increases, the average distance between the Dy^{3+} ions decreases, enhancing the interaction between them. This enhanced interaction facilitates a more efficient energy transfer between the Dy^{3+} ions. This results in the excitation energy moving through multiple Dy^{3+} ions, when photon emission occurs. In addition to Dy^{3+}–Dy^{3+} energy transfer, the presence of defects in the material serves as an additional pathway for luminescence quenching [16, 23]. These defects act as traps, capable of trapping excitation energy from neighboring Dy^{3+} ions if they are close enough. After being trapped, carriers at defect sites can relax back to the ground state through multiphonon nonradiative processes, which reduce the overall luminescence intensity of Dy^{3+} ions. As the Dy^{3+} concentration increases, the rate of energy trapping by defect centers also increases, resulting in a quenching effect.

5. Conclusion

Dy^{3+} ion-doped ZnS NCs with concentrations varying from 0.5 to 3% and sizes ranging from 4-6 nm were successfully synthesized by the wet chemical method. The study demonstrated

that both ZnS and ZnS:Dy^{3+} NCs have stable cubic structures. XRD analysis results showed an increase in lattice constant from 5.441 Åto 5.463 Åwhen Dy^{3+} concentration increased from 0-3%, indicating that Dy^{3+} ions successfully replaced the position of Zn^{2+} ions in the crystal lattice. UV-Vis absorption spectrum recorded a shift of the exciton absorption peak from 328 nm (ZnS) to 343 nm (ZnS: Dy^{3+}3%), resulting in a decrease in band gap from 4.21 eV to 3.87 eV. The PL spectrum of ZnS:Dy^{3+} NCs exhibits six characteristic emission lines, of which the 580 nm yellow peak ($^4F_{9/2} \rightarrow {}^6H_{13/2}$) is the strongest. The emission intensity increases gradually with the Dy^{3+} concentration, and fluorescence quenching occurs when the Dy^{3+} concentration increases to 2%. CIE color coordinate analysis shows a CCT shift from 16731 K (pure ZnS, cold blue) to 4910 K (ZnS: Dy^{3+}3%, warm white). Thus, by controlling the Dy^{3+} concentration, the emission spectrum can be tuned from cold blue to warm white. The fluorescence decay curve shows a decrease in the lifetime from 0.76 ms to 0.27 ms when the Dy^{3+} concentration increases from 0.5 to 3%, demonstrating the efficient energy transfer from the ZnS semiconductor substrate to the Dy^{3+} ions and the role of the cross-relaxation mechanism in the intensity distribution between the blue, yellow, and red bands. The ZnS:Dy^{3+} NCs allow for controlled tuning of the luminescence color, opening prospects for applications in white light LEDs, displays, and optical sensors.

Acknowledgement

This research is funded by the Vietnam National Foundation for Science and Technology Development (NAFOSTED) under grant number 103.02-2021.48.

Author contributions

Trinh Thi Thu Huong, Nguyen Xuan Ca: Methodology, Investigation, Manuscript writing, Supervision. Nguyen Thi Hien: Investigation, Formal analysis.

Conflict of interest

The authors have no conflict of interest to declare.

References

[1] N. X. Ca, N. D. Vinh, S. Bharti, P. M. Tan, N. T. Hien, V. X. Hoa *et al.*, *Optical properties of Ce^{3+} and Tb^{3+} co-doped ZnS quantum dots*, J. Alloys Compd. **883** (2021) 160764.

[2] S. S. Khan, J. P. Steffy, L. Sruthi, A. Syed, A. M. Elgorban, I. Abid *et al.*, *Construction of ZnS QDs decorated g-C_3N_4 nanosheets for boosting photocatalytic and anticancer activity: a novel insight*, Ceram. Int. **50** (2024) 36479.

[3] D. B. Bora, S. Das, A. Phukan, S. Kalita, P. P. Handique and R. Borah, *Brønsted–lewis acidic ionic liquid-derived ZnS quantum dots as a highly efficient and recyclable catalyst for the biginelli reaction*, Nanoscale **17** (2025) 10718.

[4] R. Pradheepa, I. Manimehan and P. Sakthivel, *Structural, bandgap tailoring, morphological and magnetic properties of Sm^{3+}-doped ZnS quantum dots*, Mater. Sci. Eng. B **306** (2024) 117463.

[5] M. Haque, I. Konthoujam, S. Lyndem, S. Koley, K. Aguan and A. S. Roy, *Formation of ZnS quantum dots using green tea extract: structural, optical and bio-imaging applications*, J. Mater. Chem. B **11** (2023) 1998.

[6] S. Murugan, M. Ashokkumar, P. Sakthivel and D. Choi, *Sulfur deficiency mediated visible emission of ZnS QDs synthesized via solvothermal route*, Heliyon **9** (2023) e17947.

[7] N. T. Hien, Y. Y. Yu, K. C. Park, N. X. Ca, T. T. K. Chi, B. T. T. Hien *et al.*, *Influence of Eu doping on the structural and optical properties of $Zn_{1-x}Eu_xSe$ quantum dots*, J. Phys. Chem. Solids **148** (2021) 109729.

[8] P. M. Tan, T. Ngoc, V. D. Nguyen, N. T. Hien, V. X. Hoa, N. X. Truong *et al.*, *Study of optical properties and energy transfer mechanism in Tb^{3+}-doped ZnS quantum dots*, Opt. Mater. **114** (2021) 110901.
[9] N. D. Vinh, P. M. Tan, P. V. Do, S. Bharti, V. X. Hoa, N. T. Hien *et al.*, *Effect of dopant concentration on structural and luminescence properties of Sm^{3+}-doped CdS quantum dots*, RSC Adv. **11** (2021) 7961.
[10] A. Kumawat, S. Chattopadhyay, R. K. Verma and K. P. Misra, *Eu doped ZnO nanoparticles with strong potential for photoluminescence and antibacterial applications*, Mater. Lett. **308** (2022) 131221.
[11] D. D. Hile, H. C. Swart, S. V. Motloung, T. E. Motaung, R. E. Kroon, K. O. Egbo *et al.*, *Synthesis and characterization of europium doped ZnSe thin films for optoelectronic applications*, Mater. Chem. Phys. **262** (2021) 124303.
[12] S. Jindal and P. Sharma, *Optical and magnetic properties of Dy^{3+} doped CdS nanoparticles*, Mater. Sci. Semicond. Process. **108** (2020) 104884.
[13] S. Ahmad, *First-principles relativistic analysis of Dy-doped CdSe: electronic structure and optical properties*, Phys. B **714** (2025) 417395.
[14] S. Sa, A. Phuruangrat, T. Thongtem and S. Thongtem, *Characterization and photocatalysis of visible-light-driven Dy-doped ZnO nanostructures*, Inorg. Chem. Commun. **117** (2020) 107944.
[15] G. El Fidha, N. Bitri, F. Chaabouni, S. Acosta, F. Güell, C. Bittencourt *et al.*, *Physical and photocatalytic properties of sprayed Dy-doped ZnO thin films prepared by ultrasonic spray pyrolysis*, RSC Adv. **11** (2021) 24917.
[16] N. Sharma and P. P. Sahay, *Solution combustion synthesis, structural and optical studies of Dy-doped ZnO nanoparticles*, J. Lumin. **257** (2023) 119655.
[17] J. Carranza, L. A. González and J. Escorcia-García, *Luminescence enhancement of Mn^{2+}-doped ZnS nanoparticles synthesized by microwave irradiation*, Ceram. Int. **51** (2025) 46268.
[18] X. Tian, J. Wen, S. Wang, J. Hu, J. Li and H. Peng, *Starch-assisted synthesis and optical properties of ZnS nanoparticles*, Mater. Res. Bull. **77** (2016) 279.
[19] H. K. Sharma, P. K. Shukla and S. L. Agrawal, *Effect of sulphur concentration on ZnS nanoparticles*, J. Mater. Sci.: Mater. Electron. **28** (2017) 6226.
[20] S. Gouraha, K. B. Masood, S. J. Gilani, A. Rai, H. S. Tewari and J. Singh, *Enhanced photoluminescence and structural properties of Dy-doped sodium zinc molybdate for photocatalytic applications*, Nanoscale Adv. **7** (2025) 3038.
[21] R. Mohan, C. Rakkappan, N. Punitha, K. Jayamoorthy, P. Magesan and N. Srinivasan, *Capping-induced changes in zn0.96ni0.04s nanoparticles: structural, optical and magnetic studies*, Chem. Phys. Impact **7** (2023) 100260.
[22] P. V. Do, L. D. Thanh, T. T. C. Thuy, N. V. Nghia, N. M. Hung, N. T. M. Thuy *et al.*, *Structure, optical properties and energy transfer of Eu^{3+}-doped cdse quantum dots synthesized by a hydrothermal route*, Ceram. Int. **51** (2025) 6616.
[23] N. T. Hien, N. T. Kien, V. H. Yen, T. Ngoc, P. V. Do, V. X. Phuc *et al.*, *Optical properties and judd–ofelt analysis of Dy^{3+}-doped $CoAl_2O_4$ nanomaterials*, Nanoscale Adv. **6** (2024) 5598.
[24] M. Salavati-Niasari, M. Ranjbar and D. Ghanbari, *A rapid microwave route for ZnS nanoparticles*, J. Nanostruct. **1** (2012) 231.
[25] M. Jothibas, S. J. Jeyakumar, C. Manoharan, I. K. Punithavathy, P. Praveen and J. P. Richard, *Structural and optical properties of ZnS nanoparticles*, J. Mater. Sci.: Mater. Electron. **28** (2017) 1889.
[26] S. Muthukumaran and M. A. Kumar, *Structural, ftir and pl properties of ZnS:Cu thin films grown by chemical bath deposition*, Mater. Lett. **93** (2013) 223.
[27] R. Gärd, Z. X. Sun and W. Forsling, *Ft-ir and ft-raman studies of colloidal zns*, J. Colloid Interface Sci. **169** (1995) 393.
[28] U. Anitha, R. Usha, A. Jithin, A. Christy and S. Varughese, *Thermal effect on band gap and photoluminescence in ZnO:Er nanostructures*, Mater. Today Proc. **3** (2016) 145.
[29] A. M. Ghaleb and A. Q. Ahmed, *Structural, electronic, and optical properties of sphalerite ZnS: a DFT study*, Chalcogenide Lett. **19** (2022) 309.